GEOPHYSICAL RESEARCH LETTERS, VOL. ???, XXXX, DOI:10.1029/,

Shear strain localization in elastodynamic rupture simulations

Eric G. Daub, M. Lisa Manning, and Jean M. Carlson

Physics Department, University of California, Santa Barbara, CA 93106, USA

We study strain localization as an enhanced velocity weakening mechanism on earthquake faults. Fault friction is modeled using Shear Transformation Zone (STZ) Theory, a microscopic physical model for non-affine rearrangements in granular fault gouge. STZ Theory is implemented in spring slider and dynamic rupture models of faults. We compare dynamic shear localization to deformation that is uniform throughout the gouge layer, and find that localized slip enhances the velocity weakening of the gouge. Localized elastodynamic ruptures have larger stress drops and higher peak slip rates than ruptures with homogeneous strain.

1. Introduction

The earthquake problem spans a vast range of length and time scales, from contacts between individual grains up through tectonic networks of faults. One of the primary modeling challenges involves identifying the relevant physical instabilities, and accurately and efficiently propagating this information between scales. In this study, we investigate gouge-scale strain localization as a physical mechanism for enhanced velocity weakening and apply it to the larger scale problem of dynamic rupture propagation on faults. Strain localization has been observed in a variety of contexts, including numerical simulations of gouge [*Morgan and Boettcher*, 1999], experimental studies of laboratory faults [*Marone*, 1998], and field observations of faults [*Chester and Chester*, 1998].

The formation of shear bands is a dynamic instability that we resolve numerically by incorporating a gouge layer of finite width. This approach differs from the common practice of implementing a slip weakening or rate and state friction law on a planar fault. In our model, the dynamic behavior of the friction law determines how strain is distributed throughout the gouge layer. Within the gouge, the material is governed by Shear Transformation Zone (STZ) Theory, a microscopic physical model for non-affine deformation in amorphous materials [*Falk and Langer*, 1998, 2000]. We study the formation of localized shear bands, in contrast with homogeneous deformation. For homogeneous deformation, strain is uniform throughout the gouge layer. In shear bands, slip spontaneously localizes to an interface which is narrow even on the scale of the gouge. The dynamic instability associated with localization enhances the velocity weakening that occurs with homogeneous deformation. We find that the enhanced weakening due to shear strain localization decreases the dynamic sliding friction and increases the peak slip rates in dynamic earthquake models. The results illustrate that gouge-scale strain localization has fault-scale consequences.

2. STZ Friction Law

STZ Theory is a continuum model for amorphous materials, suitable for predicting the larger scale constitutive behavior of a layer of fault gouge. STZ Theory captures certain features of a wide array of amorphous materials, including deformation of metallic glasses [*Falk and Langer*, 1998, 2000], boundary lubrication [*Lemaitre and Carlson*, 2004], granular flow [*Lois et al.*, 2005], shear bands in glassy systems [*Manning et al.*, 2008], and frictional weakening in dynamic earthquake rupture [*Daub and Carlson*, 2008].

A schematic of the fault is shown at the left in Fig. 1. A layer of fault gouge, which is modeled using STZ Theory, is sheared between elastic rocks. The plastic strain rate $\dot{\gamma}_{pl}$ can vary in the z-direction in the gouge (center picture in Fig. 1), though the shear stress τ is assumed to be uniform in the layer.

Non-affine rearrangements in the gouge occur in localized regions, called shear transformation zones (STZs). STZs are modeled as bistable zones that switch between two orientations under shear stress. An STZ can only flip once in the direction of the applied shear stress, so STZs are continually created and annihilated to sustain plastic flow. A schematic of an STZ switching orientation is shown at the right in Fig. 1.

The plastic strain rate is influenced by two properties of the gouge: the number of STZs, and how these STZs change orientation. The number of STZs follows a Boltzmann distribution, with an effective disorder temperature χ [*Langer*, 2004], and the STZs also change orientation due to the applied stress. These two contributions can be summarized as:

$$\dot{\gamma}_{pl} = \exp\left(-1/\chi\right) R\left(\tau\right). \tag{1}$$

The function $R(\tau)$ describes how the rate at which STZs change orientation depends on the applied shear stress. The physics behind our choice for $R(\tau)$ is an Eyring model [*Eyring*, 1936], which matches the logarithimic velocity dependence of laboratory faults. However, the enhancement of velocity weakening that strain localization produces is independent of the details of $R(\tau)$.

Regions with higher effective temperature have more STZs, and undergo more plastic strain. The effective temperature is distinct from the thermal temperature, but is similar to the free volume [*Langer*, 2007], which was used as the state variable in previous STZ friction models [*Lemaitre*, 2002]. However, we expect the effective temperature to exhibit dynamic behavior similar to thermal temperature, and we therefore include shear heating and diffusion terms in its governing partial differential equation. The friction equations and the parameters for our simulations can all be found in Table 1. The details of the derivation can be found in *Manning et al.* [2007] and *Lemaitre* [2002].

3. Spring Slider Model

To investigate the dynamics of localization, we study the STZ friction law (Table 1) coupled to a non-inertial single degree of freedom elastic slider. A layer of gouge of width $2w$ separates two blocks, one of which is pulled by a spring of stiffness k at a velocity V_0. We numerically solve for the stress and the effective temperature in the gouge layer using finite differences with an explicit two step time integration scheme. Boundary conditions on the effective temperature

0094-8276/08/$5.00

are periodic, as the effective temperature dynamics are not particularly sensitive to the boundary conditions. We drive the slider from rest to a seismic slip rate of $V_0 = 1$ m/s with a spring of stiffness $k = 100000$ MPa/m. This approximates the rapid loading and slip acceleration that occurs during dynamic seismic slip. We set the half width of the gouge layer as $w = 1$ m and start with an initial shear stress of $\tau(t = 0) = 70$ MPa.

A special case of the spring slider dynamics arises for homogeneous initial conditions for the effective temperature. In this case, by symmetry all subsequent deformation is homogeneous. We set the initial effective temperature to be uniformly $\chi(t = 0) = 0.018$. A plot of stress as a function of displacement is illustrated in Fig. 2, which shows that stress weakens with displacement in a manner similar to the laboratory-based Dieterich-Ruina friction law [*Dieterich*, 1979], and the STZ Free Volume law considered by *Daub and Carlson* [2008].

In general, we expect the initial conditions for effective temperature in the gouge to reflect the inherent heterogeneity of fault zones [*Chester and Chester*, 1998]. A localized shear band dynamically forms in this case, due to the dynamic response of the friction equations. A shear band, with a width that scales with the diffusion constant $\sqrt{D}$, develops and ultimately accomodates all of the strain in the material.

While a narrow shear band results from any non-uniform initial conditions, we focus on an idealized scenario to illustrate the dynamic evolution of the shear band. We add a small amplitude ($\Delta\chi = 2 \times 10^{-7}$) symmetric step perturbation in the center of the gouge layer of half width 0.1 m to the otherwise uniform initial effective temperature ($\chi(t = 0) = 0.018$).

We compare the shear stress as a function of displacement for both dynamically localized strain and homogeneous strain in Fig. 2(a). Uniform strain requires about 0.3 m of displacement for the shear stress to stabilize to $\tau = 63.38$ MPa. Dynamic localization drops the sliding stress to $\tau = 62.14$ MPa much more rapidly, and illustrates that localization enhances the velocity weakening of the gouge.

Figures 2(b) and 2(c) show snapshots of the strain rate in the gouge layer for dynamically localizing strain at a series of representative points along the stress versus displacement curve. During the earliest stages of displacement, strain occurs nearly uniformly throughout the gouge layer (plot (1) in Fig. 2(b)). The effect of the initial perturbation is negligible, and the strain rate is uniform. The displacement before localized strain begins depends on the magnitude of the perturbation in the initial effective temperature. This is because a region with an elevated effective temperature also has a higher strain rate (Eq. (1)). The shear heating term in the effective temperature equation (Table 1) is proportional to the strain rate, so regions of increased effective temperature heat more rapidly. Therefore, for larger initial perturbations, the local effective temperature increases more rapidly, and less displacement is needed before the strain dynamically localizes.

The strain rate profile once localization begins is shown in curve (2) in Fig. 2(b). The dynamic instability in the friction law causes strain to localize to a shear band, and friction weakens rapidly. A narrower shear band (plots (3) in Fig. 2(b) and (4) in Fig. 2(c)) develops with further displacement. By symmetry, the narrow shear band occurs in the center of the gouge, and its width is determined by the diffusion constant. Once the strain has completely localized to this diffusion-limited shear band, the frictional strength stabilizes. While the shear heating and diffusion terms do not exactly cancel each other, there is no noticeable change in the effective temperature on the time scale of an earthquake rupture and the gouge slides stably.

Table 1. Equations and parameters for the STZ constitutive law. The equations include the specific version of Eq. (1) and the partial differential equation governing the effective temperature.

Equations	
$\dot{\gamma}_{pl} = \exp(-1/\chi)\, 2\epsilon/t_0 \exp(-f_0)\,(1 - \tau_y/\tau)\cosh(\tau/\sigma_d)$	
$\partial\chi/\partial t = \dot{\gamma}_{pl}\tau/(c_0\tau_y)\left(1 - \chi\log(\dot{\gamma}_0/\dot{\gamma}_{pl})/\chi_w\right) + \dot{\gamma}_{pl} D\partial^2\chi/\partial z^2$	
Parameter	Description
$\epsilon = 10$	Typical number of particles in an STZ
$t_0 = 10^{-6}$ s	STZ rearrangement time scale
$f_0 = 118$	STZ rearrangement activation energy
$\tau_y = 50$ MPa	Yield stress (below τ_y, $\dot{\gamma}_{pl} = 0$)
$\sigma_d = 0.5$ MPa	Stress fluctuation for STZ rearrangement
$c_0 = 1$	Effective temperature specific heat
$\dot{\gamma}_0 = 80000$ s^{-1}	Strain rate at which χ diverges
$\chi_w = 0.5$	Stress weakens with strain rate if $\chi_w < 1$
$D = 10^{-5}$ m^2	Diffusion constant

4. Dynamic Ruptures

In this section, we investigate the impact of strain localization on the propagation of spontaneous elastodynamic ruptures. We model the fault gouge as a thin layer with half-width w between two homogeneous, isotropic, linear elastic solids. We solve for the elastodynamic response for 2D anti-plane slip using a spectral boundary integral method [*Perrin et al.*, 1995]. The elastodynamic equation is solved simultaneously with the friction law (Table 1).

The spectral boundary integral method can only accomodate explicit time steps. The diffusion term in the effective temperature equation imposes a time step restriction that makes implementation in a rupture code impractical. However, ignoring diffusion in the spring slider model leads to nearly the same stress response as a function of displacement. Therefore, as a first effort to incorporate localization into dynamic rupture models, we omit the diffusion term in the effective temperature evolution equation.

We consider a simple fault 2 km in length along strike, with a gouge half width of 1 m. The friction parameters in Table 1 are spatially uniform along strike and throughout the gouge width (not including the effective temperature, which we solve for dynamically). The shear stress on the fault is initially $\tau(t = 0) = 70$ MPa, except for a small patch of width 0.2 km at the center of the fault where the stress is 79 MPa to initiate rupture. We consider two different rupture scenarios, analogous to those in the spring slider section: one where shear strain localizes dynamically, and one where deformation is homogeneous. The initial effective temperature does not vary along strike, and within the gouge layer it is the same as for the corresponding spring slider model for each rupture scenario.

A plot comparing how stress weakens with slip for the two ruptures is shown in Fig. 3(a). During the initial stages of slip, the curves are indistinguishable. For the later stages of slip, shear stress weakens much more rapidly due to the dynamic instability of localization, increasing the stress drop. Homogeneous deformation and dynamic localization produce very different slip rates, as can be seen in Fig. 3(b). The rupture front arrives earlier and has a higher peak slip rate when strain localization occurs.

To illustrate the importance of the dynamic instability, we contrast our results for localized shear with two additional homogeneous ruptures of different fixed gouge widths w chosen to match particular aspects of the localized rupture. Slip velocity as a function of time is plotted at a point

0.35 km from the hypocenter for all models in Fig. 3(b). The properties that we compare are the peak slip velocity and the time at which slip initiates. The rupture front in the intermediate model ($w = 0.375$ m) matches the arrival time of the localized rupture, but the peak slip rate is smaller. For the narrowest gouge thickness ($w = 0.1$ m), we see peak slip rates similar to the localized rupture but earlier arrival. Figure 3(c) plots the slip rate as a function of slip for the homogeneous rupture with $w = 0.1$ m and the localized rupture. This clearly shows that the initial broad deformation in the localized rupture does not simply delay the rupture, but also lessens the slip acceleration during the earliest stages of slip.

5. Discussion

The main effect of dynamic strain localization in our simulations is to provide a mechanism for enhanced velocity weakening. The dynamic instability that produces localization has two effects on the shear stress: a reduced dynamic sliding stress, and a very rapid decrease in stress with slip. Allowing for enhanced weakening makes our faults more unstable – both the stress drop and the peak slip rates increase for dynamic localization relative to homogeneous slip.

The width of the narrow shear band in our simulations is determined by the diffusion length scale $\sqrt{D}$. For different driving rates, other shear band widths are possible.

Other weakening mechanisms have been discussed in the context of rapid seismic slip, including pore fluid pressurization [*Lachenbruch*, 1980], flash heating at asperity contacts [*Tullis and Goldsby*, 2003], production of a thixotropic silica gel [*Di Toro et al.*, 2004], and frictional melting [*Di Toro et al.*, 2006]. Most of these are due to (regular) thermal effects. Localization complements these, as localization occurs before significant change in the thermal temperature. Rupture models that employ both could examine how thermal weakening and shear localization interact.

The enhanced weakening effect of dynamic localization occurs regardless of the choice of the function $R(\tau)$ in Eq. (1). Other forms of $R(\tau)$ will still exhibit more rapid weakening during localized deformation. This indicates that shear localization can affect a variety of materials, and have consequences for other geophysical systems.

Acknowledgments. The authors thank Eric Dunham for providing the dynamic rupture code used in this study. This work was supported by the James S. McDonnell Foundation, the David and Lucile Packard Foundation, NSF grant number DMR-0606092, and the NSF/USGS Southern California Earthquake Center, funded by NSF Cooperative Agreement EAR-0106924 and USGS Cooperative Agreement 02HQAG0008.

References

Chester, F. M., and J. S. Chester (1998), Ultracataclasite structure and friction processes of the Punchbowl Fault, San Andreas system, California, *Tectonophysics*, *295*, 199-221.

Daub, E. G., and J. M. Carlson (2008), A constitutive model for fault gouge deformation in dynamic rupture simulations, submitted to *J. Geophys. Res.*

Dieterich, J. H. (1979), Modeling of rock friction 1. Experimental results and constitutive equations, *J. Geophys. Res.*, *84*(NB5), 2161-2168.

Di Toro, G., D. L. Goldbsy, and T. E. Tullis (2004), Friction falls towards zero in quartz rock as slip velocity approaches seismic rates, *Nature*, *427*, 436-439.

Di Toro, G., T. Hirose, S. Nielsen, G. Pennacchioni, and T. Shimamoto (2006), Natural and experimental evidence of melt lubrication of faults during earthquakes, *Science*, *311*, 647-649.

Eyring, H. J. (1936), Viscosity, plasticity, and diffusion as examples of absolute reaction rates, *J. Chem. Phys.*, *4*, 283.

Falk, M. L., and J. S. Langer (1998), Dynamics of viscoplastic deformation in amorphous solids, *Phys. Rev. E*, *57*(6), 7192-7205.

Falk, M. L., and J. S. Langer (2000), From simulations to theory in the physics of deformation and fracture, *MRS Bull.*, *25*(5), 40-45.

Falk, M. L., and Y. Shi (2002), Strain localization in a molecular-dynamics model of a metallic glass, *Mat. Res. Soc. Symp. Proc.*, *754*, CC6.20.

Lachenbruch, A. H., (1980), Frictional heating, fluid pressure, and the resistance to fault motion, *J. Geophys. Res.*, *85*(NB11), 6097-6112.

Langer, J. S. (2004), Dynamics of shear transformation zones in amorphous plasticity: Formulation in terms af an effective disorder temperature, *Phys. Rev. E*, *70*(4), 041502.

Langer, J. S. (2007), Shear-transformation-zone theory of plastic deformation near the glass transition, arxiv:0712.0399v1.

Langer, J. S., and M. L. Manning (2008), Steady-state, effective-temperature dynamics in a glassy material, *Phys. Rev. E*, *76*, 056107.

Lemaitre, A. (2002), Rearrangements and dilatancy for sheared dense materials, *Phys. Rev. Lett.*, *89*(19), 195503.

Lois, G., A. Lemaitre, and J. M. Carlson (2005), Numerical tests of constitutive laws for dense granular flows, *Phys. Rev. E*, *72*, 051303.

Manning, M. L., J. S. Langer, and J. M. Carlson (2007), Strain localization in a shear transformation zone model for amorphous solids, *Phys. Rev. E*, *76*(5), 056106.

Marone, C. (1998), Laboratory-derived friction laws and their application to seismic faulting, *Ann. Rev. Earth Planet. Sci.*, *26*, 643-696.

Morgan, J. K., and M. S. Boettcher (1999), Numerical simulation of granular shear zones using the distinct element method - 1. Shear zone kinematics and the micromechanics of localization, *J. Geophys. Res.*, *104*(B2), 2703-2720, doi:10.1029/1998JB900056.

Perrin, G., J. R. Rice, and G. Zheng (1995), Self-healing slip pulse on a frictional surface, *J. Mech. Phys. Solids*, *43*, 1461-1495.

Shi, Y., M. B. Katz, H. Li, and M. L. Falk (2007), Evaluation of the disorder temperature and free-volume formalisms via simulations of shear banding in amorphous solids, *Phys. Rev. Lett.*, *98*, 185505.

Tullis, T. E., and D. L. Goldsby (2003), Flash melting of crustal rocks at almost seismic slip rates, *Eos Trans. AGU*, *84*(46), Fall Meet. Suppl. Abstract S51B-05.

E. G. Daub, M. L. Manning, and J. M. Carlson Physics Department, Broida Hall, University of California, Santa Barbara, CA 93106, USA. (edaub@physics.ucsb.edu)

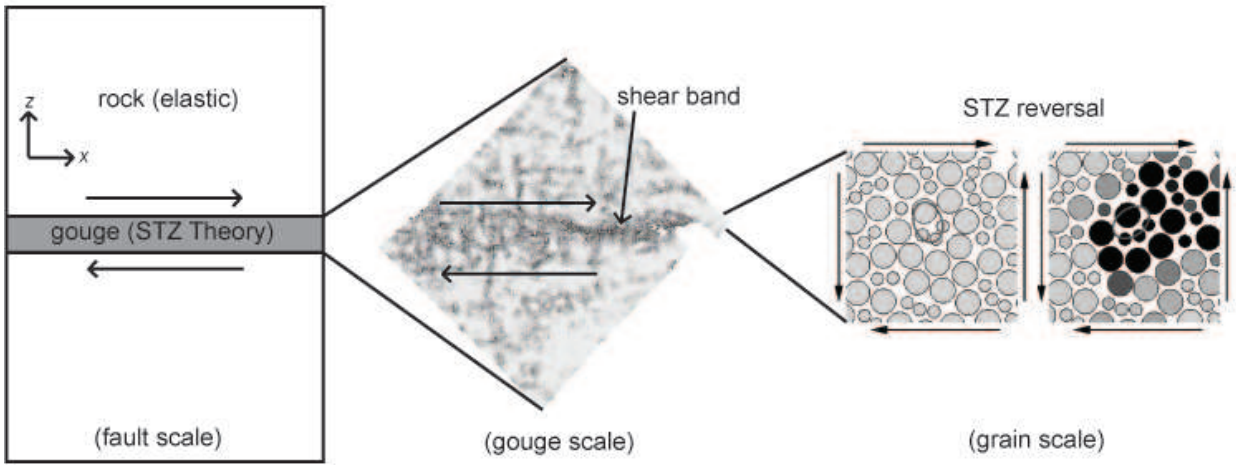

Figure 1. An illustration of the range of scales in the earthquake rupture problem. The scale moves to progressively smaller phenomena from left to right. Left: fault scale model, with a thin layer of gouge described by STZ theory sheared between elastic rocks. Center: close up of deformation inside the gouge, where shear strain develops into a localized shear band (dark regions). Shear band image taken from *Falk and Shi* [2002], and re-oriented to match the sense of shear of the fault and grains. Right: microscopic picture of the grain scale, with an STZ undergoing transformation from a "+" oriented zone (left) to a "−" oriented zone (right). As the gouge deforms plastically, the ellipse drawn through the particles flips its orientation. STZ diagram taken from *Falk and Langer* [1998].

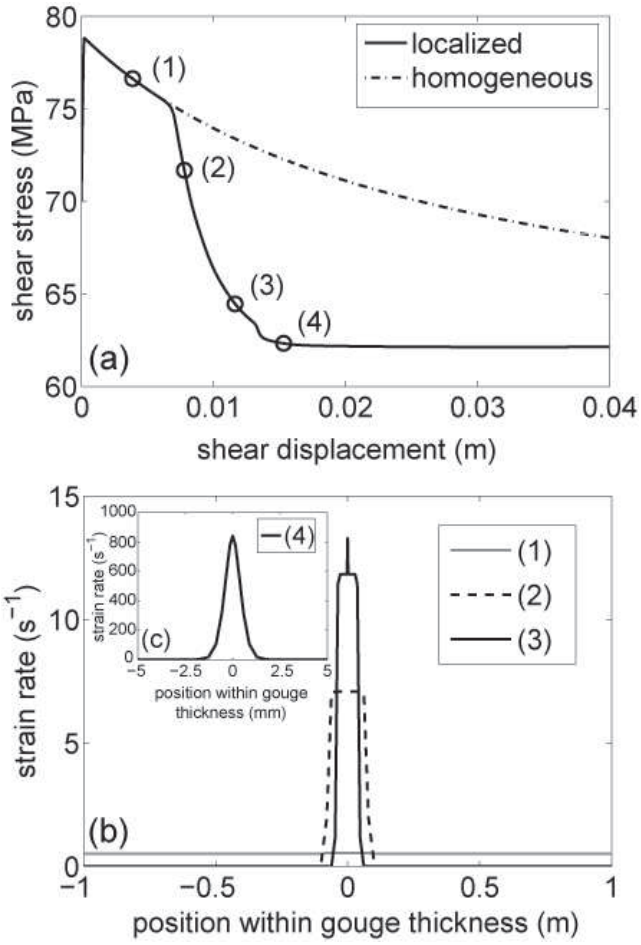

Figure 2. (a) Plot of shear stress as a function of shear displacement for the spring slider model. Comparison between dynamic strain localization and homogeneous deformation reveals that localized strain exhibits more rapid weakening. (b) Strain rate profiles for four representative shear displacements during localized strain, indicated in plot (a). (1) An initial period of broad deformation occurs before (2) strain dynamically localizes. (3) A narrower, diffusion-limited shear band develops with further shear. (c) Inset: The narrow shear band eventually accommodates all of the deformation.

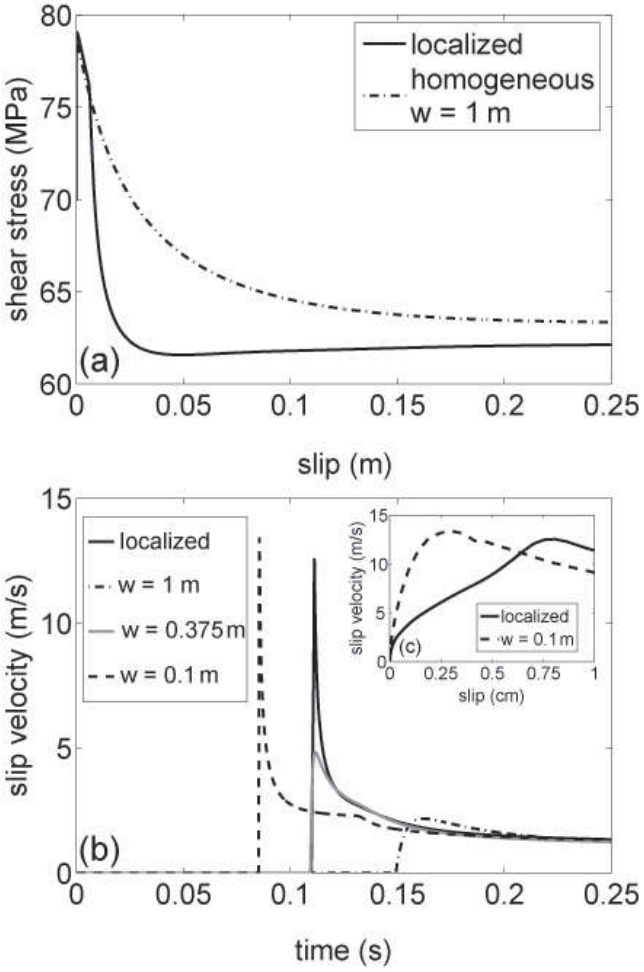

Figure 3. Dynamic rupture evolution at a point 0.35 km from the hypocenter. (a) Comparison of shear stress as a function of slip. Dynamic localization of deformation produces more rapid velocity weakening than the rupture with homogeneous strain. (b) Plot of slip rate as a function of time. The dynamic strain localization rupture is compared with a host of models with homogeneous strain. None of the values of the imposed gouge width w can match both the peak slip rate and rupture front arrival of the rupture with localized strain. (c) Inset: Slip rate as a function of slip for the localized and narrowest width homogeneous rupture. The more rapid acceleration of slip in the narrowest homogeneous rupture is distinct from the localized model.